Dyes and Pigments 93 (2012) 1538–1543

Contents lists available at ScienceDirect

Dyes and Pigments

journal homepage: www.elsevier.com/locate/dyepig

Short communication

Synthesis, spectral properties and DFT/TDDFT study on novel methyl heteroazulene derivative

P. Gąsiorski [a], K.S. Danel [b], M. Matusiewicz [a], T. Uchacz [c], A.V. Kityk [a,*]

[a] Faculty of Electrical Engineering, Częstochowa University of Technology, Al. Armii Krajowej 17, 42-200 Częstochowa, Poland
[b] Department of Chemistry, University of Agriculture, Balicka str. 122, 30-149 Kraków, Poland
[c] Faculty of Chemistry, Jagiellonian University, Ingardena str. 3, 30-060 Kraków, Poland

ARTICLE INFO

Article history:
Received 22 May 2011
Received in revised form
20 July 2011
Accepted 22 July 2011
Available online 30 July 2011

Keywords:
Optical absorption spectra
Fluorescence spectra
DFT and TDDFT calculations
Annulated heteroazulene dyes
Polarizable continuum model (PCM)
Solvatochromism

ABSTRACT

Paper introduces new heteroazulene derivative, 10-methoxy-6-methyl-6*H*-5,6,7-triazadibenzo[*f*,*h*]naphtho[3,2,1-*cd*]azulene (MMTNA), including chemical aspects of its synthesis likewise optical absorption and fluorescence spectra measured in several organic solvents of different polarity. The obtained experimental results are subjected to the quantum-chemical analysis based on DFT/TDDFT/PCM calculations at the B3LYP/6-31+G(d,p) level of theory. MMTNA demonstrates insignificant solvatochromism of both first absorption and fluorescence bands caused mainly by a weakly polar feature of its ground and lowest excited states. Despite this the emission bands appears to be considerably red shifted with respect to relevant first absorption bands resulting thus to a substantial Stokes shift. Its origin is dominated by the conformational relaxation in the excited state whereas the solvent relaxation has practically no influence on the emission spectra. Low sensitivity to the host environment makes MMTNA dye perspective for a number of applications, particularly in those cases when a high stability of the emission wavelength (color) is demanded.

1. Introduction

Recent advances in the organic chemistry synthesis have resulted in appearing a series of new low and medium weight organic compounds, among which the heteroazulenes [1,2] as promising materials for electroluminescent [3–6] or biotechnological [2] applications. The annulated heteroazulene derivatives may be obtained from phenyl containing pyrazoloquinolines being known as highly efficient blue fluorescence emitters which have already found their application in single layer organic-light-emitting diodes (OLEDs) [7,8]. The seven-membered cyclization of pyrazoloquinolines into regioisomers of heteroazulenes provides a significant red shift of both excitation and emission spectra [3–6] thus eventual fundamental interest to such phenomena is also accompanied by practical needs in novel efficient fluorescent emitters in the blue–green–yellow region of the visible spectra. In such context one of key problems in OLED development remains a reduction of number of active layers [9] likewise a set of red, green, and blue emitters with high efficiency, color purity, and stability establishing of which is a matter of full-color display technology [10–12].

In this paper we introduce another new derivative of heteroazulene, 10-methoxy-6-methyl-6*H*-5,6,7-triazadibenzo[*f*,*h*]naphtho[3,2,1-*cd*]azulene (hereafter MMTNA) with the chemical structure as shown below:

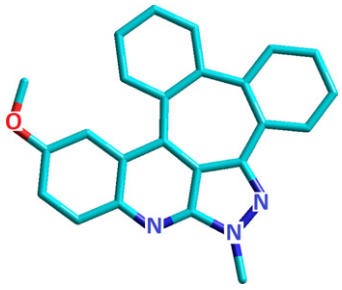

Its molecular structure is characterized by non-planar distortion of the cyclized aromatic rings imposed by steric hindrance of interacting hydrogen atoms. Despite of our previous studies on several 6-phenyl heteroazulene derivatives [3–6], MMTNA does not contain phenyl radical(s) singly bonded to heteroazulene moiety. Accordingly, its electronic transitions, as will be ascertained below, are prominently of a local type with small ground and excited state dipole moments what considerably reduces eventual solvatochromic effects and makes such

* Corresponding author.
E-mail address: kityk@ap.univie.ac.at (A.V. Kityk).

0143-7208/$ – see front matter © 2011 Elsevier Ltd. All rights reserved.
doi:10.1016/j.dyepig.2011.07.014

dye practically insensitive to a host environment. We present here the synthesis details regarding MMTNA, optical absorption and fluorescence spectra likewise the quantum-chemical analysis of the excitation and emission processes based on the density functional theory (DFT) and its time-dependent counterpart, TDDFT calculations. One must be noticed that in recent years DFT/TDDFT methods have increasingly been used [13–15] to fill the gap between simple semi-empirical and high-level ab initio calculations, particularly due to their applicability to larger molecular systems [15].

2. Synthesis, experimental and calculation procedure

General routines concerning the synthesis of heterocycles dyes are presented in Ref. [1]. Particularly for MMTNA they are specified by scheme below (Scheme 1).

Commercially available reagents (Aldrich, Fluka, Merck) were used without further purification. ^{1}H NMR and ^{13}C NMR were recorded using a Mercury-Vx 300 MHz Varian, operating at 300 MHz and 75 MHz, in $CDCl_3$ with tetramethylsilane (TMS) as an internal standard. Melting points were measured on a MELT-Temp and are uncorrected. Elementary analyses were performed on a Perkin–Elmer 2400 CHN analyzer.

2.1. 4-(2-Chlorophenyl)-6-methoxy-1-methyl-3-phenyl-1H-pyrazolo[3,4-b]quinoline (4)

Equimolar (16 mmol) amounts of p-anisidine **1**, 2-chloro benzaldehyde **2** and 1-methyl-3-phenyl-5-pyrazolone **3** were heated to reflux in ethylene glycol (20 mL). After cooling, MeOH was added and the mixture was refluxed for 30 min. The precipitate was filtered off. Pyrazoloquinoline was obtained in a pure form after column chromatography (Al_2O_3/chloroform). Yield 2.55 g (38%); yellow solid; mp = 199–201 °C; R_f = 0.62 (toluene/EtOAc; 3:1); ^{1}H NMR ($CDCl_3$, 300 MHz) δ 3.71 (*s*, 3H, OMe), 4.32 (*s*, 3H, Me), 6.80 (*d*, 1H, J = 3.0 Hz), 7.02–7.16 (*m*, 7H), 7.21–7.30 (*m*, 1H), 7.34 (dt, 1H, J = 7.8, 0.6 Hz), 7.45 (dd, 1H, J = 9.3, 3.0 Hz), 8.09 (*d*, 1H, J = 9.6 Hz); 13C NMR ($CDCl_3$, 300 MHz) δ 33.95, 55.27, 103.04, 113.61, 123.38, 124.38, 126.38, 127.25, 127.37, 128.73, 129.43, 129.80, 129.91, 131.69, 132.67, 133.67, 134.43, 138.60, 144.03, 145.11, 149.99, 155.67; Anal. Calcd. for $C_{24}H_{18}ClN_3O$; C, 72.09; H, 4.54; N,10.51; found: C, 71.92; H, 4.38; N, 10.62.

2.2. 10-methoxy-6-methyl-6H-5,6,7-triazadibenzo[f,h]naphtho[3,2,1-cd]azulene (5)

4 (1.0 g, 2.5 mmol), powdered KOH (4.2 g, 75 mmol) and quinoline (20 mL) were refluxed for 2 h. After cooling water (100 mL) and toluene (100 mL) were added. The mixture was vigorously stirred for 30 min. The water phase containing potassium salt of carbostyril was discarded. To remove residual quinoline the organic phase was extracted with 4 M HCl (2 × 50 mL) and washed with water (2 × 50 mL). After drying ($MgSO_4$), the solvent was removed on a rotary evaporator. The residue was chromatographed (Al_2O_3/$CHCl_3$). The fractions collecting the pure product were concentrated and MeOH was added dropwise. The product was collected after precipitation. Yield 0.65 g (65%); deep yellow solid; mp = 229–231 °C; R_f = 0.58 (toluene/EtOAc; 3:1); ^{1}H NMR ($CDCl_3$, 300 MHz) δ 3.89 (*s*, 3H, OMe), 4.22 (*s*, 3H, Me), 7.34–7.50 (*m*, 5H), 7.70 (dd, 1H, J = 7.8, 1.5 Hz), 7.76–7.79 (*m*, 2H), 7.98–8.01 (*m*, 2H), 8.12–8.16 (*m*, 1H); ^{13}C NMR ($CDCl_3$, 300 MHz) δ 34.10, 55.52, 105.12, 120.10, 121.95, 123.46, 126.72, 127.43, 128.18, 128.58, 129.36, 129.91, 132.18, 132.75, 134.28, 135.66, 135.75, 137.93, 140.25, 141.09, 141.53, 147.09, 150.82, 155.48; Anal. Calcd. for $C_{24}H_{17}N_3O$; C, 79.32; H, 4.72; N,11.56; found: C, 79.24; H, 4.48; N, 11.60.

The optical absorption spectra were recorded in solutions with concentration of MMTNA dye of about 10^{-5} M using several organic solvents of different polarity, i.e. weakly polar cyclohexane (CHX), medium polar tetrahydrofuran (THF) and highly polar acetonitrile (ACN). The measurements were performed by means of Shimadzu UV–VIS 2101 scanning spectrophotometer in the range of 230–600 nm using a standard 1 cm path length quartz cuvette for absorption spectrometry. The steady state photoluminescence measurements were performed using a conventional spectrofluorimeter with cooled photomultiplier EMI 955 8B operating in a single photon counting mode. For the fluorescence excitation the Hg-source (λ = 405 nm) was applied. The fluorescence spectra were corrected for the spectral sensitivity of the detecting system. The fluorescence lifetimes were estimated from the decay curves measured by time-resolved single photon counting. As an excitation source a picosecond diode laser (λ = 400 nm, τ = 70 ps pulse duration) from IBH-UK was used. Further details regarding the spectroscopic measurements can be found in Ref. [3–6].

The DFT/TDDFT calculations have been performed within the quantum-chemical package of programs Gaussian-09 [16] using B3LYP exchange correlation potential with the standard 6-31+G(d,p) basis set. Despite the overall popularity of the hybrid B3LYP potential in the organic chemistry several serious problems and critical remarks were addressed in respect to this method [17]. It turned out that an application of B3LYP may lead to a severe underestimation of excitation energies in the charge transfer states [18] and, in general, its performance considerably drops down with increased system size [19,20]. For this reason further brief justification in account of the chosen quantum-chemical method seems to be desirable here. Our recent quantum-chemical calculations on the organic systems similar to MMTNA, particularly seven-membered heteroazulene derivatives [21] likewise their five-membered counterparts, biphenyl azafluoranthene dyes [22], have revealed that DFT/TDDFT methods with the hybrid B3LYP potential give indeed quite accurate estimations of their excitation spectra. The spectral position of the first absorption band has been predicted in these heterocyclized dyes with an accuracy better than 0.02–0.05 eV. Moreover, in combination with polarizable continuum models (PCMs) B3LYP gives also a proper sign and a reasonable magnitude for the solvatochromic shift which is another evidence for the reliability of evaluated ground and excited state properties, particularly the dipole moments relevant to these states. In the case of heteroazulenes or azafluoranthenes a considerable efficiency of B3LYP calculations is likely caused by a moderate molecular size of these

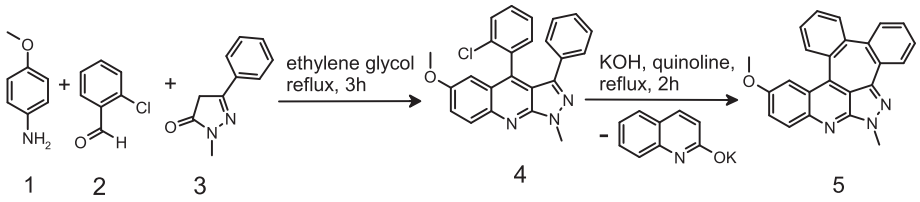

Scheme 1.

dyes as well as by preferably a local character of their low energy electronic transitions, i.e. without an evident charge separation upon the excitation. This presumably explains good accuracy of B3LYP method exhibited in previous calculations [21,22] likewise justifies its applicability to other similar heterocyclized organic dyes, especially if one deals with even a bit simpler molecular structures, e.g. MMTNA. To account the solvation the DFT/TDDFT methods were combined with PCM using linear-response (hereafter PCM-LR) or state-specific (PCM-SS) approaches available in Gaussian-09. Further details regarding these methods are given elsewhere, see e.g. Ref. [23,24], review article [25] and references in.

3. Results and discussion

Fig. 1(a) shows the equilibrium ground state geometry of the MMTNA molecule optimized by DFT in the gas phase. Similarly to other heteroazulene derivatives it is characterized by bent shape of its heteroazulene skeleton due to steric hindrance of interacting hydrogen atoms. The overall shape of the molecule as well as the bond lengths change insignificantly (less than 0.001 Å) with the solvent polarity. Fig. 1(b) and (c) present the LUMO and HOMO orbitals, respectively, calculated in the gas phase and consequently reproduced by means of the program Gabedit [26]. The HOMO → LUMO transition at the vertical excitation, exhibits only a local rearrangement of electron density without its evident separation what is a characteristic feature for purely local electronic transitions. The calculations by DFT method give the energies of the HOMO and LUMO levels, −5.37 eV and −2.25 eV, respectively, with the energy gap of 3.12 eV.

Fig. 2(a) shows the optical absorption spectra of MMTNA measured in different solvents. Its first absorption band is slightly structured due to strongly overlapped vibronic bands. In the CHX solution the first absorption maximum is centered at about 451.5 nm, but the electronic 0 → 0′ transition, associated with the HOMO–LUMO gap, should be indeed assigned to the kink-like shoulder observed at about 472 nm at the red wing of this band, see marked by the arrow in insert of Fig. 2(a) and Table 1. As the solvent polarity rises from CHX to THF the first absorption maximum, likewise the electronic 0 → 0′ transition, both exhibit a weak red shift just on a few nanometers although further rising of the solvent polarity, from THF to ACN, keeps their spectral positions practically unchanged. Such solvatochromic behavior appears to be consistent with further quantum-chemical analysis. In particular, the DFT/TDDFT analysis gives for the singlet ground state, S_0, and the lowest excited state, S_1, relatively small values of the relevant dipole moments, $\mu_g = \mu(S_0) = 2.61$ D and $\mu_e = \mu(S_1) = 1.74$ D what explains a weak solvatochromism exhibiting by MMTNA dye in the optical absorption (Fig. 2(a)) and fluorescence (Fig. 3(a)) spectra.

Fig. 2(b) presents the optical absorption spectra calculated within TDDFT/PCM-LR approach. The blue, green and red online colors correspond here to CHX, THF and ACN solutions, respectively. The vertical lines of relevant colors correspond to the oscillator strengths due to the electronic transitions between the singlet ground and excited states. The continuous lines simulate the absorption spectra where relevant bands are approximated by the Gaussian function with the parameter of the band shape broadening, Γ, equals 0.25 eV. Other details regarding the methodology of such calculations may be found in Ref. [27–31]. Comparing Fig. 2(a) and Fig. 2(b) one can see that DFT/TDDFT/PCM-LR method well reproduces the basic features of the measured spectra including the first absorption band in the visible range and the strongest absorption band in the UV-region centered at about of 250 nm. However, the first absorption maximum, being calculated for several solvents, appears to be somewhat red shifted, particularly on about of 20 nm with respect to the measured ones. Evidently, such discrepancy must not be only attributed to the accuracy of DFT/TDDFT calculations but also to the fact that a vibronic coupling indeed has been ignored in such calculations. One must be emphasized that the spectral position of the first absorption band in Fig. 2(b) indeed corresponds to 0 → 0′-transition whereas the absorption maximum in the region of 451–454 nm in Fig. 2(a) is relevant with 0 → 1′-transition being obviously blue shifted with respect to the 0→0′-transition by approximately of a single vibronic spacing. Accordingly, the shape just of the first absorption band is more properly defined in insert of Fig. 2(b) by its modeling via the vibronic series similarly as in Ref. [32–34]. The absorbance is defined here as $\propto E\sum_{j=0}^{\infty}(e^{-S}S^j/j!)\exp[-(E-E_{00'}-jE_v)^2/(4h_0k_BT)]$, where S is the vibronic coupling constant, $E = h\nu$ is the excitation energy, E_v is the

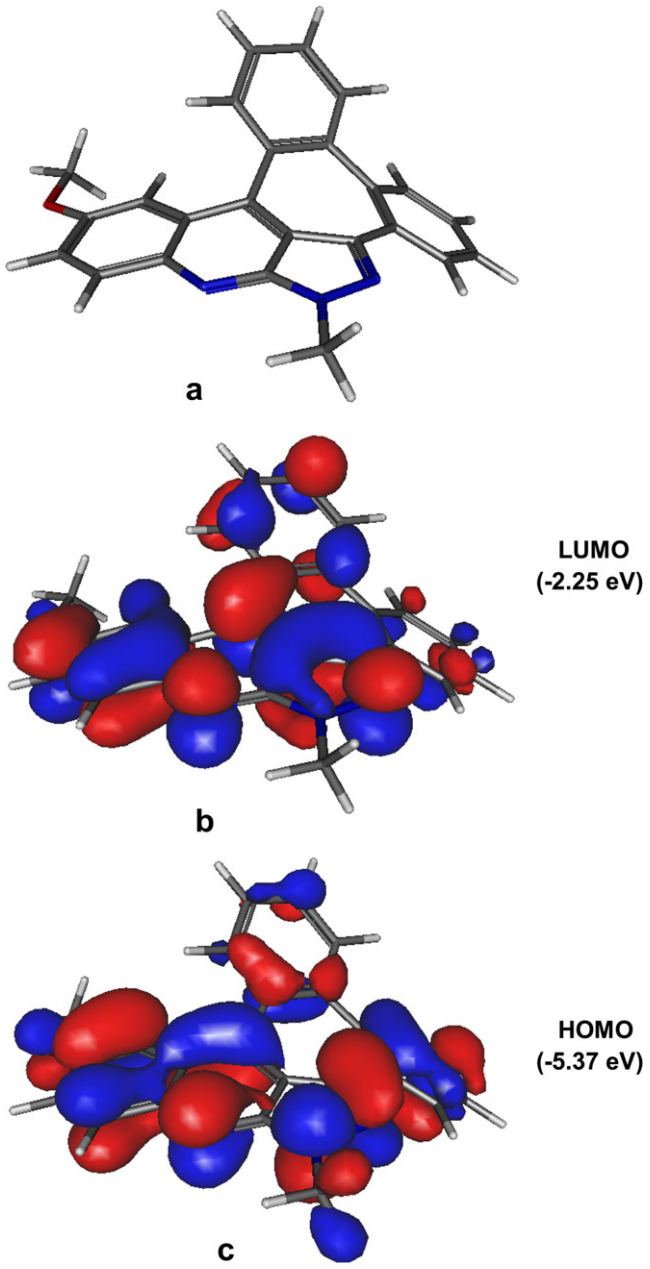

Fig. 1. Ground state equilibrium geometry of MMTNA molecule (a), LUMO (b) and HOMO (c) orbitals as calculated by DFT method in the gas phase.

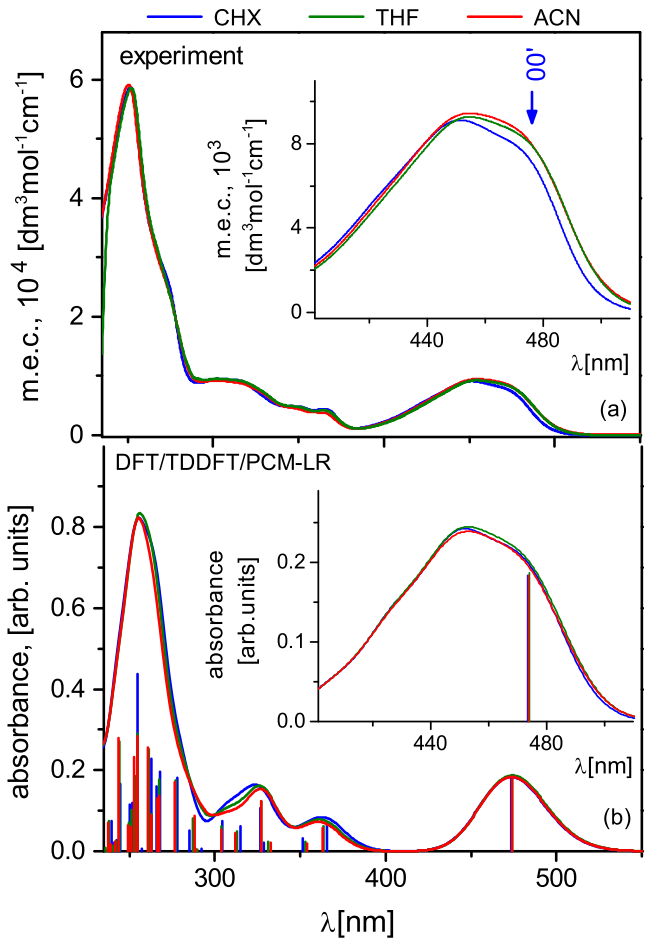

Fig. 2. The optical absorption spectra of MMTNA. Section (a) shows the measured spectra in CHX (blue online color), THF (green online color) and ACN (red online color) solutions; insert shows the first absorption band in details. Section (b) shows the spectra calculated by DFT/TDDFT/PCM-LR in CHX (blue color online), THF (green online color) and ACN (red online color) solutions. The vertical lines are the oscillator strengths corresponding to the electronic transitions between the ground and excited singlet states ($\Gamma = 0$); the continuous lines simulate the optical absorption spectra by introducing the Gaussian band shape broadening ($\Gamma = 0.25$ eV). The insert in Section (b) shows the first absorption band calculated in CHX, THF and ACN solutions by DFT/TDDFT/PCM-LR method with the band shape defined by the set of the model parameters: $S = 1.1$, $E_v = 1120$ cm^{-1} and $h_n = 0.095$ eV (see text for corresponding details). (For interpretation of the references to color in this figure legend, the reader is referred to the web version of this article.)

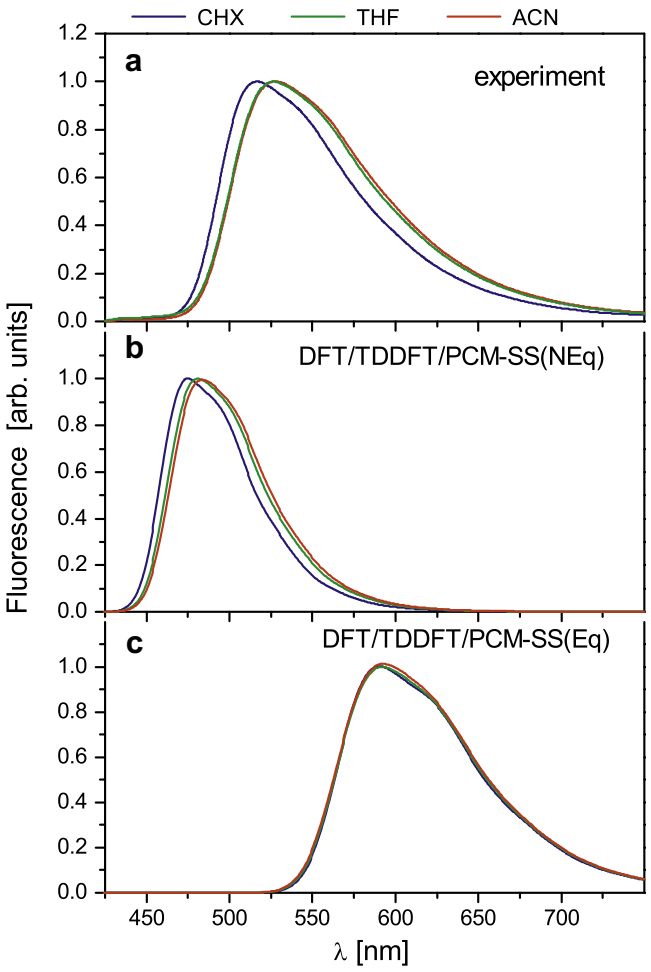

Fig. 3. The fluorescence spectra of MMTNA in CHX (blue color online), THF (green color online) and ACN (red color online) solutions. Section (a) shows the measured fluorescence spectra. Section (b) and Section (c) present the spectra calculated within the TDDFT/PCM-SS(NEq) and TDDFT/PCM-SS(Eq) approaches, respectively. The band shape is defined here by the set of the model parameters: $S = 0.95$, $E_v = 1120$ cm^{-1} and $h_n = 0.095$ eV, see text for description. (For interpretation of the references to color in this figure legend, the reader is referred to the web version of this article.)

vibronic energy spacing, k_B is the Boltzmann constant, T is the temperature. The reorganization energy h_0 is related to the low-frequency motions such as reorientation of the solvent shell (h_s) as well as any other low-frequency and medium-frequency nuclear motions of the solute (h_n). Following [32] it may be given by their superposition, i.e. $h_0 = h_n + h_s = h_n + (\vec{\mu}_e - \vec{\mu}_g)^2 a_0^{-3}[(\varepsilon - 1)/(2\varepsilon + 1) - (n^2 - 1)/(2n^2 + 1)]$, where a_0 is the Onsager (cavity) radius, ε and n are the static dielectric constant and the refractive index of the solvent, respectively. In such spectra simulations the values S, E_v and h_n are considered as the model (fit) parameters. With the magnitudes $S = 1.1$, $E_v = 1120$ cm^{-1} (0.139 eV) and $h_n = 0.095$ eV one gets the best agreement with the shape of the first absorption band being measured in solvents of different polarity. The vibronic spacing, E_v with the effective frequency of 1120 cm^{-1} appears in the range of 1100–1500 cm^{-1} which according to the vibrational analysis corresponds to modes consisting of stretching vibrations, C–C, C–N or N–N bonds that form heteroazulene skeleton. Other quantities, like transition energy $E_{00'}$, the ground state dipole moment $\vec{\mu}_g$ and the excited state dipole moment $\vec{\mu}_e$ have been directly determined within the DFT/TDDFT or DFT/TDDFT/PCM-LR calculations. The Onsager radius, a_0, is taken to be equal 0.527 nm as suggested by the molecular volume calculation within the DFT method. By comparing inserts in Fig. 2(a) and Fig. 2(b) it is obvious that within such approach the DFT/TDDFT/PCM-LR method practically perfectly reproduces the shape of the first absorption band likewise the basic features of its solvatochromic behavior. Table 1, compares the transition energies $E_{00'}$ as being determined from the measured spectra and calculated within the DFT/TDDFT/PCM-LR and DFT/TDDFT/PCM-SS approaches. In both cases the discrepancy between the experiment and theory is about of 0.01 eV or less. The

Table 1
Excitation 0 → 0′ energies of MMTNA being determined from the measured absorption spectra and calculated by TDDFT/PCM-LR and TDDFT/PCM-SS methods.

$E_{00'}^{abs}$: Solvent	Experiment [eV]	PCM-LR [eV]	PCM-SS [eV]
CHX	2.63	2.619	2.633
THF	2.62	2.615	2.632
ACN	2.62	2.617	2.633

difference is that the DFT/TDDFT/PCM-LR approach slightly underestimates the excitation energy whereas the DFT/TDDFT/PCM-SS one vice versa.

Fig. 3(a) shows the normalized steady state fluorescence spectra measured in the solvents of different polarity. Similarly to the optical absorption the fluorescence spectra are slightly structured due to vibronic coupling and are characterized by a weak bathochromic (red) shift while the solvent polarity rises. In all the cases the emission maximum nearly coincides with the electronic $0' \rightarrow 0$ transition. Table 2 lists the wavelength of emission maximum (λ_m^{fl}), the fluorescence quantum yield (Φ_{fl}) and the fluorescence lifetime (τ_{fl}) being determined within the fluorescence decay measurements by using the time-resolved single photon counting method. Other photophysical constants such as the radiationless (k_{nr}) and radiative (k_{fl}) rate constants likewise the fluorescence momentum (M_{fl}) have been evaluated using a simple kinetic model of an irreversible excited charge transfer state formation [32]. While the solvent polarity changes from CHX to ACN the fluorescence momentum of MMTNA dyes deviates within about of 10% suggesting thus that the electronic properties of the states associated with the fluorescence emission should not change significantly with the solvent polarity. Despite of weak solvatochromism accompanying the fluorescence spectra of MMTNA dye, its emission band appears to be considerably red shifted with respect to the first absorption band resulting thus to a Stokes shift. Depending on solvent polarity it ranges from 65 to 73 nm. Evidently, the origin of the Stokes shift is dominated here by the conformational relaxation in the excited state rather than a solvent relaxation. Already in the gas phase it provides a substantial red shift of the emission band. Corresponding excitation and emission energies, $E_{00'}^{gs}$ and $E_{0'0}^{gs}$, can be indeed estimated in the gas phase applying Onsager reaction field theory [35–37], particularly by extrapolating the spectral positions of the optical absorption and emission bands into the region of zero solvent polarity $F=(\varepsilon - 1)/(2\varepsilon + 1) - (n^2 - 1)/(4n^2 + 2)$, i.e. in the limit $F \rightarrow 0$, see Fig. 4. The difference $\Delta E_{a-f}^{o} = E_{00'}^{gs} - E_{0'0}^{gs}$, gives in this case a rough idea about the conformational changes accompanying the absorption–emission cycle. Analyzing the experimental data one obtains $\Delta E_{a-f}^{o} \approx 0.21$ eV. In the following we compare this value with the results of quantum-chemical calculations. Fig. 3(b) and (c) show the normalized steady state fluorescence spectra calculated in the solvents of different polarity within the TDDFT/PCM-SS(NEq) and TDDFT/PCM-SS(Eq) models, respectively. Herein both models are based on the same state-specific approach, available in Gaussian-09, which deal with either equilibrium (Eq) or non-equilibrium (NEq) conformations in the excited state. In particular, the DFT/TDDFT/PCM-SS(NEq) method calculates the emission spectra for the molecular structure being optimized in the ground state by DFT/PCM method with the solvation reaction field corresponding to the lowest excited state of the solute. This type of calculations indeed corresponds to the case of the equilibrium solvation but non-equilibrium solute geometry. To some extent it may be considered as crude and/or artificial approach which, nevertheless, allows to understand an influence of the solvent reorganization on

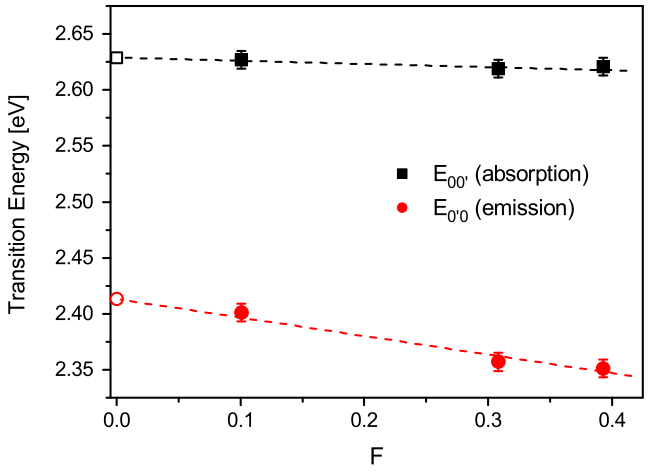

Fig. 4. Transition energies $E_{00'}$ (absorption) and $E_{0'0}$ (emission) vs solvent polarity F as derived from the measured spectra (solid symbols). Open symbols corresponds to the transition energies for the gas phase, $E_{00'}^{gs}$ and $E_{0'0}^{gs}$, being obtained by an extrapolation of $E_{00'}(F)$ and $E_{0'0}(F)$ dependences into the region $F \rightarrow 0$.

the electronic transitions separating it from the effects caused by a solute reorganization in polar environment. On the other hand, the TDDFT/PCM-SS(Eq) method represents one of the standard approaches where the molecular structure optimization in the excited state and the fluorescent spectra calculation are performed within the same TDDFT/PCM-SS method. It is the case when the solvent reaction field and the solute geometry in the excited state both reach fully relaxed states before subsequent vertical electronic transition into the final non-equilibrium ground state. One must be emphasized that TDDFT/PCM-SS calculations provide in both cases only the emission energy, associated with $0' \rightarrow 0$-transition, likewise the ground and/or excited state dipole moments. A real shape of the fluorescence bands due to vibronic coupling have been reproduced similarly as for the optical absorption, namely like in [32–34], i.e. $\propto E^3 \sum_{j=0}^{\infty}(e^{-S}S^j/j!)\exp[-(E - E_{0'0} + jE_v)^2/(4h_0k_BT)]$ with the set of the quantities being already described above. The shape of fluorescence band may be well reproduced with the following model parameters $S = 0.95$, $E_v = 1120$ cm^{-1} and $h_n = 0.095$ eV. Nevertheless, the spectral positions of the calculated emission bands remain a subject for further discussion. Table 3 lists the emission energies representing the maxima of the measured fluorescence spectra [section (a)] as well as calculated within TDDFT/PCM-SS(NEq) [section (b)] or TDDFT/PCM-SS(Eq) [section (c)] approaches. Comparing Fig. 3(b) and Fig. 3(a) we conclude that TDDFT/PCM-SS(NEq) method overestimates the emission energies on about of 0.23–0.25 eV. One may found such discrepancy quite obvious keeping in mind that this type of calculations ignores, by a definition, the solute relaxation in the excited state which plays a dominant role in the observed Stokes shift as has been ascertained above. Simple extrapolation of the emission energy $E_{0'0}(F)$, calculated by TDDFT/PCM-SS(NEq), into the region $F \rightarrow 0$ and its

Table 2
The photophysical constants of MMTNA dye obtained in the CHX, THF and ACN solutions. λ_m^{abs} is the absorption maxima, $\lambda_{00'}^{abs}$ is wavelength corresponding to $0 \rightarrow 0'$-transition, λ_m^{fl} is the fluorescence maxima, Φ_{fl} is the fluorescence quantum yield, τ_{fl} is the fluorescence lifetime, k_{nr} is the radiationless rate constant, k_{fl} is the radiative rate constant and M_{fl} is the fluorescence moment.

Solvent	$\lambda_m^{abs}(\lambda_{00'}^{abs})$ [nm]	λ_m^{fl} [nm]	Φ_{fl}	τ_{fl} [ns]	k_{nr} [10^7 s^{-1}]	k_{fl} [10^7 s^{-1}]	M_{fl} [D]
CHX	451.5 (472.0)	516.5	0.44	13.8	4.06	3.19	2.20
THF	454.0 (473.5)	526.0	0.48	13.2	3.94	3.63	2.46
ACN	454.0 (473.0)	527.5	0.32	14.1	4.82	2.27	2.09

Table 3
Emission 0′ → 0 energies of MMTNA being determined from the measured fluorescence spectra and calculated by TDDFT/PCM-SS(NEq) and TDDFT/PCM-SS(Eq) methods.

$E^{fl}_{0'0}$: Solvent	Experiment [eV]	PCM-SS(NEq) [eV]	PCM-SS(Eq) [eV]
CHX	2.40	2.633	2.119
THF	2.36	2.606	2.118
ACN	2.35	2.594	2.119

comparison with the excitation energy $E_{00'}(F = 0)$, as obtained in a similar way by TDDFT/PCM-SS method, results to nearly zero value for ΔE^{o}_{a-f} in the gas phase. Contrary to this, TDDFT/PCM-SS(Eq) method a bit underestimates the emission energy, namely on about of 0.22–0.28 eV, likewise the magnitude ΔE^{o}_{a-f} which turns out to be equal 0.51 eV. Importantly, the direct calculation of ΔE^{o}_{a-f} in the gas phase by TDDFT method gives rather close its magnitude to this value, 0.53 eV. The discrepancy between experiment and theory of that type, but even larger in magnitude has been revealed recently also in other heterocyclized organic dyes [21,22]. This fact means that the TDDFT optimization in the excited state provides the conformational changes which appear to be somewhat stronger than they are in reality. As an alternative reason for such discrepancy could also be the emission from the excited state being far from equilibrium. However, MMTNA exhibits quite long relaxation times of the fluorescence emission, 13–14 ns (see Table 2), which evidently are sufficient to reach new equilibrium in the excited state. More reliable interpretation should refer rather to the quality of the excited state geometry optimization which is less accurate than in the case of the ground state geometries provided by DFT optimization. Such opinion has been shared in the recent discussion with official representatives of the Gaussian Inc. [38]. Nevertheless, both state-specific approaches indicate that the solvent reorganization in the excited state is indeed weak and has only a marginal meaning what appears to be also consistent with the experimental observation. Such conclusion directly follows from a weak solvatochromism demonstrated by MMTNA dye due to a weakly polar feature of its lowest excited state.

4. Conclusion

In conclusion, we have introduced here new heteroazulene derivative, MMTNA dye, including the chemical aspects of its synthesis, the optical absorption and fluorescence spectra measured in several organic solvents as well as the quantum-chemical analysis of the spectroscopic properties based on DFT/TDDFT/PCM calculations at the B3LYP/6-31+G(d,p) level of theory. The DFT/TDDFT/PCM calculations quite well reproduce the basic features of the measured absorption spectra, particularly the strongest absorption band in the UV-region and the first absorption band in the visible range. Both the linear-response and state-specific approaches quite precisely predict the spectral position of the first absorption band in solvents of different polarity; the discrepancy between the experiment and theory is about of 0.01 eV. As for the fluorescence emission being considered the TDDFT calculations somewhat underestimate the transition energy. Depending on a solvent polarity corresponding discrepancy ranges from 0.22 to 0.28 eV and should be attributed to the accuracy of the TDDFT optimization in the excited state. MMTNA demonstrates insignificant solvatochromism of both first absorption and fluorescence bands caused mainly by a weakly polar feature of its ground and lowest excited states. Despite this, the emission bands appears to be considerably red shifted with respect to the first absorption bands resulting thus to a Stokes shift which depending on solvent polarity ranges from 65 to 73 nm. The origin of the Stokes shift is dominated by the conformational relaxation in the excited state whereas the solvent relaxation has practically no influence on the emission spectra. Low sensitivity to the host environment makes MMTNA dye to be perspective for a number of applications, particularly in those cases when a high stability of the emission wavelength (color) is demanded.

Acknowledgment

The calculations have been carried out in Wrocław Centre for Networking and Supercomputing (http://www.wcss.wroc.pl), grant No 160.

Appendix. Supplementary material

Supplementary data related to this article can be found online at doi:10.1016/j.dyepig.2011.07.014.

References

[1] Danel KS, Wisła A, Uchacz T. ARKIVOC 2009;Part 10:71.
[2] Hirama Y, Minakawa N, Matsuda A. Bioorg Med Chem 2011;19:352.
[3] Danel KS, Gąsiorski P, Matusiewicz M, Całus S, Uchacz T, Kityk AV. Spectrochim Acta A 2010;77:16.
[4] Całus S, Danel KS, Uchacz T, Kityk AV. Mater Chem Phys 2010;121:477.
[5] Gąsiorski P, Danel KS, Matusiewicz M, Uchacz T, Kityk AV. J Lumin 2010;130:2460.
[6] Gąsiorski P, Danel KS, Matusiewicz M, Uchacz T, Vlokh R, Kityk AV. J Fluoresc 2011;21:443.
[7] Całus S, Gondek E, Danel A, Jarosz B, Pokladko M, Kityk AV. Mater Lett 2007;61:3292.
[8] Gondek E, Całus S, Danel A, Kityk AV. Spectrochim Acta A 2008;69:22.
[9] He Z, Kan C-W, Ho C-L, Wong W-Y, Chui C-H, Tong K-L, et al. Dyes Pigm 2011;88:333.
[10] Mao G, Orita A, Fenenko L, Yahiro M, Adachi C, Otera J. Mater Chem Phys 2009;115:378.
[11] Cheng J-A, Chen CH, Shieh H-PD. Mater Chem Phys 2009;113:1003.
[12] Huang J, Xu B, Lam M-K, Cheah K-W, Chen CH, Su J-H. Dyes Pigm 2011;89:155.
[13] Lunak JS, Vynuchala J, Valac M, Havel L, Hrdina R. Dyes Pigm 2009;82:102.
[14] Guillaumont D, Nakamura S. Dyes Pigm 2000;46:85.
[15] Fabian J. Dyes Pigm 2010;84:36.
[16] Frisch MJ, Trucks GW, Schlegel HB, Scuseria GE, Robb MA, Cheeseman JR, et al. Gaussian 09, revision B.01. Wallingford CT: Gaussian, Inc.; 2010.
[17] Wong BM, Hsieh TH, Chem J. Theory Comput 2010;6:3704.
[18] Kurashige Y, Nakajima T, Kurashige S, Hirao K, Nishikitani Y. J Phys Chem A 2007;111:5544.
[19] Dreuw A, Head-Gordon M. J Am Chem Soc 2004;126:4007.
[20] Wodrich MD, Corminboeuf C, Schreiner PR, Fokin AA, Schleyer PvR. Org Lett 2007;9:1851.
[21] Gąsiorski P, Danel KS, Matusiewicz M, Uchacz T, Kuźnik W, Piątek Ł, et al. submitted for publication, Mater Chem Phys.
[22] Gąsiorski P, Danel KS, Matusiewicz M, Uchacz T, Kuźnik W, Kityk AV. J Fluoresc, in press, doi: 10.1007/s10895-011-0932-1.
[23] Improta R, Barone V, Scalmani G, Frisch MJ. J Chem Phys 2006;125:054103.
[24] Improta R, Scalmani G, Frisch MJ, Barone V. J Chem Phys 2007;127:074504.
[25] Tomasi J, Mennucci B, Cammi R. Chem Rev 2005;105:2999.
[26] Allouche AR. J Comput Chem 2011;32:174.
[27] Całus S, Gondek E, Danel A, Jarosz B, Kityk AV. Opt Commun 2006;268:64.
[28] Całus S, Gondek E, Danel A, Jarosz B, Kityk AV. Opt Commun 2007;271:16.
[29] Całus S, Gondek E, Pokladko M, Kulig E, Jarosz B, Kityk AV. Spectrochim Acta A 2007;67:1007.
[30] Gondek E, Danel A, Kwiecień B, Nizioł J, Kityk AV. Mater Chem Phys 2010;119:140.
[31] Koścień E, Gondek E, Pokladko M, Jarosz B, Vlokh RO, Kityk AV. Mater Chem Phys 2009;114:860.
[32] Kapturkiewicz A, Herbich J, Karpiuk J, Nowacki J. J Phys Chem A 1997;101:2332.
[33] Marcus RA. J Phys Chem 1989;93:3078.
[34] Gould IR, Young RH, Miller LJ, Albrecht AC, Farid SJ. J Am Chem Soc 1994;116:8188.
[35] Onsager L. J Am Chem Soc 1936;58:1486.
[36] Lippert E. Z Naturforsch A 1955;10:541.
[37] Mataga N, Kaifu Y, Koizumi M. Bull Chem Soc Jpn 1955;28:690.
[38] Clemente FR. Private communication. Technical Support Gaussian, Inc.; 31.03.2011.